Efficient Large Spectral Collocation Method for MHD Laminar Natural Convection Flow from a Vertical Permeable Flat Plate with Uniform Surface Temperature, Soret, Dufour, Chemical Reaction and Thermal Radiation

Titilayo Morenike Agbaje, Sandile Sydney Motsa, Peter Leach, and Precious Sibanda

Abstract—**In this work, the three-dimensional steady natural convection boundary layer flow of an electrically conducting and viscous incompressible fluid is studied. The coupled nonlinear partial differential equations that describe the flow have been solved using a recently developed large parameter spectral perturbation method (LSPM). This method has not been used before in the literature to obtain numerical solutions of three dimensional MHD laminar natural convection flow with Soret and Dufour effects. The partial differential equations that defines the problem under investigation are highly coupled and nonlinear. Hence they cannot be solved analytically using series-based methods. Indeed, validation of this numerical method for general fluid flows, or heat and mass transfer problems has not yet been done. This work explores and evaluates the accuracy and robustness of the large parameter spectral perturbation in finding solutions of coupled nonlinear partial differential equations.**

Index Terms—**Natural convection, Magnetohydrodynamics (MHD), thermal radiation, Soret and Dufour, Large parameter spectral perturbation method.**

I. Introduction

MAGNETOHYDRODYNAMIC (MHD) is one which combines fluid mechanics and electromagnetism, that is, how an electrically conducting fluid behaves in the presence of a magnetic and electric field. In many engineering and industrial processes, the study of magnetohydrodynamic natural convection flow and heat transfer have diverse applications which found its uses in, for example, nuclear reactors, MHD generator, MHD pumps, flight MHD, MHD flowmeters, MHD accelerators, geothermal extractions, plasma studies, boundary layer control in the field of aeronautics and aerodynamics. Another great importance of MHD natural convection boundary layer flow past a permeable surface is in space flight and in a nuclear reactor. This applications usually involves a strong magnetic field and a low-density gas and as a result, the Hall current and ion slip becomes immensely important.

The natural convection boundary layer flow of an electrically conducting fluid in the presence of a magnetic field has been discussed by many authors. Mention may be made of the research of Yamanishi [1] who investigated the Hall Effect in the viscous flow of ionized gas through straight channels. Sing and Cowling [2] derived similarity solutions and solutions based on a Pohlhausen-like type of approximation of thermal convection in a magnetohydrodynamic boundary layer. The numerical method of Nactsheim-Swigert shooting iteration technique together with Runge-Kutta six order iteration scheme has been used by Wahiduzzaman et al. [3] to solve the system of governing non-similar equations describing the flow of MHD convection and mass transfer flow of viscous incompressible fluid about an inclined plate with Hall current and constant heat flux. In their study, it was assumed that the induced magnetic field is negligible when compared with the imposed magnetic field. Seth et al. [4], [5] investigated Hall effects on unsteady MHD natural convection flow of a heat absorbing fluid past an accelerated moving vertical plate with ramped temperature and effects of Hall current and rotation on unsteady MHD natural convection flow with heat and mass transfer past an impulsively moving vertical plate in the presence of radiation and chemical reaction, respectively. In their studies, the exact solutions are obtained in closed form by Laplace transform technique under the Boussinesq approximation. Saha et al [7] considered the effect of Hall current on the MHD laminar natural convection flow from a vertical permeable flat plate with uniform surface temperature, where it was assumed that the induced magnetic field is negligible compared to the imposed magnetic field. The transformed governing partial differential equations were solved using the regular perturbation method for small transpiration parameter, asymptotic solutions are obtained for large transpiration rate, the local non-similarity method and implicit finite difference method together with Keller box scheme for any transpiration rate. The finite difference method, the local non-similarity method and the perturbation method were used by Saha et al. [8] to analyze the effect of Hall current on MHD natural convection flow from a vertical permeable flat plate with uniform heat flux.

Manuscript received April 18, 2019; revised October 30, 2019. This work was supported by the National Research Foundation of South Africa under (Grant number: 116661), the Durban University of Technology, and the University of KwaZulu-Natal, South Africa.

Titilayo Morenike Agbaje is with the Institute of Systems Science, Durban University of Technology, P O Box 1334, Durban 4000, South Africa, and the School of Mathematics,Statistics and Computer Sciences, University of KwaZulu-Natal, Private Bag X01 Scottsville 3209, Pietermaritzburg, South Africa e-mail: titilayoagbaje@gmail.com.

Sandile Sydney Motsa is with the University of Swaziland, Private Bag 4, Kwaluseni, Matsapha M201, Swaziland

Peter Leach is with the Institute of Systems Science, Durban University of Technology, P O Box 1334, Durban 4000, South Africa

Precious Sibanda is with the School of Mathematics,Statistics and Computer Sciences, University of KwaZulu-Natal, Private Bag X01 Scottsville 3209, Pietermaritzburg, South Africa

The problem investigated is that of MHD laminar natural convection flow from a vertical permeable flat plate with uniform surface temperature, chemical reaction and thermal radiation and is defined by a coupled system of four nonlinear partial differential equations. The model is an extension of that investigated by Saha et al. [7] to incorporate mass, thermal radiation, heat generation, chemical reaction, Soret and Dufour effects on the flow. The model in the absence of the mass, thermal radiation, heat generation, chemical reaction, Soret and Dufour effects has earlier been solved by Saha et al. [7] the perturbation method, local non-similarity method and an implicit finite difference method together with Keller-box scheme. The perturbation method, local non-similarity method and implicit finite method has been used extensively by many researchers on related problems defined on large parameter intervals (see, for example, Mahmood et al. [9], Hussain et al. [10], Hossain et al. [11]). The perturbation method is an analytic technique for finding approximate solutions to differential equations. It has been observed by previous researchers who used the perturbation method to obtain series solutions about a large perturbation parameter that higher order perturbation equations may be impossible or difficult to solve exactly beyond a certain order of approximation. This yields less accurate results if one, two or three perturbation approximation is used to obtain approximate solutions. Hence, there is a need to generate higher order perturbation approximations. Besides, there are limits to how far the perturbation series analytic approach can be used in solving nonlinear systems of partial differential equations involving many coupled equations. This is because nonlinear systems of partial differential equations involving many coupled equations are difficult to solve analytically. The implicit finite difference method is a known numerical method used by many researchers for solving nonlinear partial differential equations defined on large parameter intervals. The implicit finite difference method was introduced by Cebeci and Bradshaw [12]. The finite difference schemes are known to require many grid points to achieve good accuracy. Hence, a lot of computer memory and computational time may be needed to obtain accurate results.

The aim of this study is to therefore demonstrate the applicability of the large parameter spectral perturbation method on coupled systems of nonlinear partial differential equations which have the Soret and Dufour effects and are defined over a large parameter interval and cannot be solved analytically even with methods that look for series solutions. To the best of the authors' knowledge, series approaches akin to the LSPM have not been reported in the literature for solving coupled nonlinear partial differential equations modelling MHD laminar natural convection flow. This study presents the first opportunity to evaluate the robustness and accuracy of the LSPM in finding solutions of coupled systems of nonlinear partial differential equations describing MHD laminar natural convection flow from a vertical permeable flat plate with uniform surface temperature, Soret, Dufour, chemical reaction and thermal radiation effects. The LSPM is a combination of both the analytical and numerical solution techniques. In the LSPM, we construct a series solution about a large perturbation parameter and the Chebyshev spectral collocation method is used to solve the resulting series equations numerically. In this current study, it was observed that the sequence of ordinary differential equations which are derived from the series expansion are coupled and cannot be solved analytically, hence, the introduction of the Chebyshev spectral collocation method to resolve the resulting series equations numerically. With the use of the Chebyshev spectral collocation method, it will be possible to gain approximate numerical solutions of the higher order perturbation equations which are impossible to obtain analytically due to the nature of the problem considered in this study. To establish the accuracy of the LSPM, approximate numerical solutions obtained using the LSPM are validated using the multi-domain bivariate spectral quasilinearisation method (MD-BSQLM) and published results in the literature, and our results are found to be in an excellent agreement. The MD-BSQLM is a numerical method that combines the quasilinearisation idea together with the Chebyshev spectral collocation and bivariate Lagrange interpolation. In the MD-BSQLM, the nonlinear systems of partial differential equations are first linearized using the quasilinearization method of Bellman and Kalaba [13]. The resulting equations are then integrated into multiple sub-intervals using the Chebyshev spectral collocation method. The numerical results from this study show that the LSPM is accurate and can be utilised as an alternative numerical tool for solving coupled nonlinear systems of partial differential equations defined over large parameter domain and cannot be solved analytically using analytical methods. The advantage of the LSPM is that unlike other numerical methods, it applies discretization only in the space (η)-direction when solving a partial differential equation. This feature enables the LSPM to compute approximate numerical solutions in a very efficient and computationally fast manner. To further establish the accuracy of the LSPM, the residual error and the solution error of the differential equation will be shown. Simulations will be carried out to show pertinent flow characteristics such as the local skin-friction coefficient, local Nusselt number, local Sherwood number, velocity, heat, and mass transfer rates.

II. Mathematical Formulation

We investigate a steady natural convection boundary layer flow of an electrically conducting and viscous incompressible fluid from a semi-infinite heated permeable flat plate in the presence of a transverse magnetic field and thermal radiation with the effects of Hall currents, chemical reaction, Soret and Dufour. The $x-$ axis is along the vertically upward direction, while the $y-$ axis is normal to it and away from the plate surface. The leading edge of the permeable surface is taken as coincident with $z-$axis. The plate temperature is assumed to be non-uniform and depending on the distance x measured from the leading edge of the plate while the ambient temperature is maintained at uniform temperature T_∞ and concentration C_∞. Furthermore, we consider a uniform mass flux, V_0 through the permeable vertical surface of the plate. The Hall current effect gives rise to a force in that direction. Hence, the flow becomes three-dimensional. The flow configuration and the flow coordinate system are shown in Fig. 1. Under the usual boundary layer approximation, the flow is governed by the following equations (see [7]),

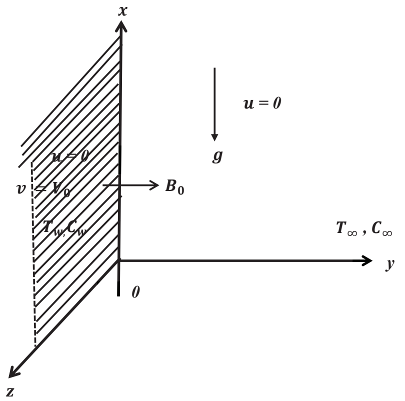

Fig. 1. The flow coordinate system and the flow configuration

$$\frac{\partial u}{\partial x}+\frac{\partial v}{\partial y}=0, \quad (1)$$

$$u\frac{\partial u}{\partial x}+v\frac{\partial u}{\partial y}=\nu\frac{\partial^2 u}{\partial y^2}+g\beta(T-T_\infty)-\frac{\sigma B_0^2}{\rho(1+m^2)}\left(u+mw\right), \quad (2)$$

$$u\frac{\partial w}{\partial x}+v\frac{\partial w}{\partial y}=\nu\frac{\partial^2 w}{\partial y^2}+\frac{\sigma B_0^2}{\rho(1+m^2)}\left(mu-w\right), \quad (3)$$

$$u\frac{\partial T}{\partial x}+v\frac{\partial T}{\partial y}=\alpha\frac{\partial^2 T}{\partial y^2}+\frac{D_m k_T}{c_s c_p}\frac{\partial^2 C}{\partial y^2}-\frac{1}{\rho c_p}\frac{\partial q_r}{\partial y} + \frac{Q_0}{\rho c_p}\left(T-T_\infty\right), \quad (4)$$

$$u\frac{\partial C}{\partial x}+v\frac{\partial C}{\partial y}=D_m\frac{\partial^2 C}{\partial y^2}+\frac{D_m k_T}{T_m}\frac{\partial^2 T}{\partial y^2}-K_r(C-C_\infty). \quad (5)$$

In the above equations, u, v and w are the velocity components along x, y and z axis, ν is the kinematic coefficient of viscosity, g is the acceleration due to gravity, β is the thermal expansion coefficient, T is the fluid temperature, T_∞ is the ambient fluid temperature, σ is the electric conductivity of the fluid, B_0 is the applied magnetic field, ρ is the fluid density, $m=(\omega^2\tau^2)$ is the Hall parameter, with ω being the cyclotron frequency of the electron, and τ as the collision time of electrons with ions, $\alpha(=\frac{\kappa}{\rho c_p})$ is the thermal diffusivity with κ being the fluid thermal conductivity and c_p the specific heat at constant pressure of the fluid, D_m is the mass diffusivity, k_T is the thermal diffusivity ratio, c_s is the concentration susceptibility, q_r is the radiative heat flux, Q_0 is the heat generation constant, T_m is the mean fluid temperature, K_r is the chemical reaction coefficient, C is the fluid concentration and C_∞ is the ambient fluid concentration. The radiative heat flux q_r is defined using the Rosseland approximation [14] as:

$$q_r=-\frac{4\sigma^*}{3k^*}\frac{\partial T^4}{\partial y}, \quad (6)$$

where σ^* and k^* are the Stefan-Boltzmann constant and mean absorption coefficient, respectively. Assuming that the temperature differences within the flow are sufficiently small, T^4 may be approximated in Taylor series form about T_∞, after ignoring higher order terms as:

$$T^4\approx 4T_\infty^3 T-3T_\infty^4. \quad (7)$$

The boundary conditions are:

$$\begin{aligned}&u(x,y)=0,\quad v(x,y)=-V_0,\quad w(x,y)=0,\quad T(x,y)=T_w,\\ &C(x,y)=C_w \quad \text{at} \quad y=0,\\ &u(x,y)=0,\quad w(x,y)=0,\quad T(x,y)=T_\infty,\\ &C(x,y)=C_\infty \quad \text{at} \quad y=\infty.\end{aligned} \quad (8)$$

In equation (8), V_0 is the transpiration velocity. When V_0 is positive, it denotes suction or withdrawal and a negative V_0 stands for injection or blowing of fluid through the permeable surface. In this present investigation the case of suction or withdrawal will only be considered rather than the blowing case and therefore, V_0 is taken to be positive throughout this study. The following dimensionless transformations for the dependent and independent variables that valid for the natural convection flow from the vertical surface are then introduced:

$$\begin{aligned}&\psi(x,y)=\nu Gr_x^{1/4}\left[f(\xi,\eta)+\xi\right],\quad \eta=\frac{y}{x}Gr_x^{1/4},\quad \xi=\frac{xV_0}{\nu}Gr_x^{-1/4},\\ &w(x,y)=\frac{\nu}{x}Gr_x^{1/2}g(\xi,\eta)\quad \theta(\xi,\eta)=\frac{T-T_\infty}{T_w-T_\infty}=\frac{T-T\infty}{\Delta T},\\ &\phi(\xi,\eta)=\frac{C-C_\infty}{C_w-C_\infty},\end{aligned} \quad (9)$$

where ψ is the stream function defined by;

$$u=\frac{\partial\psi}{\partial y},\quad v=-\frac{\partial\psi}{\partial x}, \quad (10)$$

which satisfies the continuity equation (1). In equation (9), f is the dimensionless stream function, g is the dimensionless velocity in the $z-$direction, $Gr_x=\frac{g\beta\Delta T}{\nu^2}x^3$ is the local Grashof number, θ is the dimensionless temperature of the fluid, $\Delta T=T_w-T_\infty$, ϕ is the dimensionless concentration of the fluid, η is the pseudo-similarity variable, ξ is the transpiration parameter depending on the transpiration velocity V_0 and the axial variable x. Substituting the transformations given in equation (9) into equations (2) - (5) gives the following set of non-similarity system of partial differential equations which are expressed in dimensionless form as:

$$f'''+\frac{3}{4}ff''-\frac{1}{2}f'^2+\xi f''+\theta-\frac{M}{1+m^2}(f'+mg) =\frac{1}{4}\xi\left[f'\frac{\partial f'}{\partial\xi}-f''\frac{\partial f}{\partial\xi}\right], \quad (11)$$

$$g''+\frac{3}{4}fg'-\frac{1}{2}f'g+\xi g'-\frac{M}{1+m^2}(g-mf') =\frac{1}{4}\xi\left[f'\frac{\partial g}{\partial\xi}-g'\frac{\partial f}{\partial\xi}\right], \quad (12)$$

$$\frac{1}{Pr}\left(1+N_R\right)\theta''+\frac{3}{4}f\theta'+\xi\theta'+Df\phi''+He\theta =\frac{1}{4}\xi\left[f'\frac{\partial\theta}{\partial\xi}-\theta'\frac{\partial f}{\partial\xi}\right], \quad (13)$$

$$\frac{1}{Sc}\phi''+\frac{3}{4}f\phi'+\xi\phi'-\delta\phi+Sr\theta''=\frac{1}{4}\xi\left[f'\frac{\partial\phi}{\partial\xi}-\phi'\frac{\partial f}{\partial\xi}\right]. \quad (14)$$

The boundary conditions (8) becomes,

$$\begin{aligned}&f(\xi,0)=0,\quad f'(\xi,0)=0,\quad f'(\xi,\infty)=0,\\ &g(\xi,0)=0,\quad g(\xi,\infty)=0,\\ &\theta(\xi,0)=1,\quad \theta(\xi,\infty)=0,\\ &\phi(\xi,0)=1,\quad \phi(\xi,\infty)=0.\end{aligned} \quad (15)$$

In the above equations, prime denotes differentiation with respect to η, M is the magnetic field number, Pr is the Prandtl number, N_R is the thermal radiation parameter, Df is the Dufour number, and He is the heat generation parameter, Sc is the Schmidt number, δ is the chemical reaction parameter and Sr is the Soret number. These parameters are mathematically defined as:

$$\begin{aligned}&M=\frac{\sigma B_0^2x^2}{\rho\nu Gr_x^{1/2}},\quad Pr=\frac{\nu\rho c_p}{\kappa},\quad N_R=\frac{16\sigma^* T_\infty^3}{3k^*\kappa},\\ &Df=\frac{D_m k_T(C_w-C_\infty)}{c_s c_p\nu(T_w-T_\infty)},\quad He=\frac{Q_0x^2}{\rho c_p\nu Gr_x^{1/2}},\\ &Sc=\frac{\nu}{D_m},\quad Sr=\frac{D_m k_T(T_w-T_\infty)}{T_m\nu(C_w-C_\infty)},\quad \delta=\frac{K_r x^2}{\nu Gr_x^{1/2}}.\end{aligned} \quad (16)$$

The physical quantities of interest are the local skin-friction coefficient C_{fx}, the local Nusselt number Nu_x and the local Sherwood number Sh_x, and are defined respectively by the following expressions as:

$$C_{fx}Gr_x^{-3/4} = f''(\xi,0), \quad Nu_xGr_x^{-1/4} = -\theta'(\xi,0),$$
$$Sh_xGr_x^{-1/4} = -\phi'(\xi,0). \tag{17}$$

III. LARGE PARAMTER SPECTRAL PERTURBATION METHOD (LSPM)

In this section, we derive the asymptotic solution of equations (11) - (14) subject to the boundary conditions (15) when the transpiration parameter ξ is large. When ξ is large, the dominant terms in equation (11) are f''' and $\xi f''$, g'' and $\xi g'$ in (12), θ'' and $\xi\theta'$ in (13), and ϕ'' and $\xi\phi'$ in (14). It is sufficient to balance these terms in magnitude. Therefore, given that $\theta = O(1)$ as $\xi \to \infty$, it is necessary to find appropriate scaling for f and η. Balancing the order of magnitude of f''', $\xi f''$ and θ' in equation (11), g'' and $\xi g'$ in (12), θ'' and $\xi\theta'$ in (13) and ϕ'' and $\xi\phi'$ in (14) using the method of dominant balance, it is found that $\eta = O(\xi^{-1})$, $f = O(\xi^{-3})$, $g = O(\xi^{-2})$, $\theta = O(1)$ and $\phi = O(1)$ as $\xi \to \infty$. Accordingly, we introduce the following transformations that are valid for large values of ξ as:

$$f = \xi^{-3}F(\xi,\bar{\eta}), \quad g = \xi^{-2}G(\xi,\bar{\eta}) \quad \theta = \Theta(\xi,\bar{\eta}),$$
$$\phi = \Phi(\xi,\bar{\eta}) \quad \bar{\eta} = \xi\eta. \tag{18}$$

Substituting equation (18) into equations (11) - (14) gives:

$$F''' + F'' + \Theta - \frac{M}{1+m^2}\xi^{-2}\left[F' + mG\right] = \frac{1}{4}\xi^{-3}\left[F'\frac{\partial F'}{\partial \xi} - F''\frac{\partial F}{\partial \xi}\right], \tag{19}$$

$$G'' + G' - \frac{M}{1+m^2}\xi^{-2}\left[G - mF'\right] = \frac{1}{4}\xi^{-3}\left[F'\frac{\partial G}{\partial \xi} - G'\frac{\partial F}{\partial \xi}\right], \tag{20}$$

$$\left(\frac{1+N_R}{Pr}\right)\Theta'' + \Theta' + \xi^{-2}He\Theta + Df\Phi'' = \frac{1}{4}\xi^{-3}\left[F'\frac{\partial \Theta}{\partial \xi} - \Theta'\frac{\partial F}{\partial \xi}\right], \tag{21}$$

$$\frac{1}{Sc}\Phi'' + \Phi' - \xi^{-2}\delta\Phi + Sr\Theta'' = \frac{1}{4}\xi^{-3}\left[F'\frac{\partial \Phi}{\partial \xi} - \Phi'\frac{\partial F}{\partial \xi}\right], \tag{22}$$

where prime denotes differentiation with respect to $\bar{\eta}$.

The corresponding boundary conditions are:

$$\begin{aligned}
&F(\xi,0) = 0, \quad F'(\xi,0) = 0, \quad F'(\xi,\infty) = 0,\\
&G(\xi,0) = 0, \quad G(\xi,\infty) = 0,\\
&\Theta(\xi,0) = 1, \quad \Theta(\xi,\infty) = 0,\\
&\Phi(\xi,0) = 1, \quad \Phi(\xi,\infty) = 0.
\end{aligned} \tag{23}$$

Since ξ is large, we seek solutions to equations (19) - (22) using the perturbation series approach. The functions $F(\xi,\bar{\eta})$, $G(\xi,\bar{\eta})$, $\Theta(\xi,\bar{\eta})$ and $\Phi(\xi,\bar{\eta})$ are expanded in powers of ξ^{-2} as:

$$F(\xi,\bar{\eta}) = \sum_{k=0}^{\infty}\xi^{-2k}F_k(\bar{\eta}), \quad G(\xi,\bar{\eta}) = \sum_{k=0}^{\infty}\xi^{-2k}G_k(\bar{\eta}),$$
$$\Theta(\xi,\bar{\eta}) = \sum_{k=0}^{\infty}\xi^{-2k}\Theta_k(\bar{\eta}), \quad \Phi(\xi,\bar{\eta}) = \sum_{k=0}^{\infty}\xi^{-2k}\Phi_k(\bar{\eta}). \tag{24}$$

Substituting equation (24) into equations (19) - (22) and then equating the coefficients of like powers of ξ, we obtain the equation for $k = 0$ as:

$$F_0''' + F_0'' + \Theta_0 = 0, \tag{25}$$
$$G_0'' + G_0' = 0, \tag{26}$$
$$\left(\frac{1+N_R}{Pr}\right)\Theta_0'' + \Theta_0' + Df\Phi_0'' = 0, \tag{27}$$
$$\frac{1}{Sc}\Phi_0'' + \Phi_0' + Sr\Theta_0'' = 0, \tag{28}$$

subject to the following boundary conditions

$$\begin{aligned}
&F_0(\xi,0) = 0, \quad F_0'(\xi,0) = 0, \quad F_0'(\xi,\infty) = 0,\\
&G_0(\xi,0) = 0, \quad G_0(\xi,\infty) = 0,\\
&\Theta_0(\xi,0) = 1, \quad \Theta_0(\xi,\infty) = 0,\\
&\Phi_0(\xi,0) = 1, \quad \Phi_0(\xi,\infty) = 0.
\end{aligned} \tag{29}$$

The equations for $k = 1$ are obtained as:

$$F_1''' + F_1'' + \Theta_1 - \frac{M}{1+m^2}\left[F_0' + mG_0\right] = 0, \tag{30}$$
$$G_1'' + G_1' - \frac{M}{1+m^2}\left[G_0 - mF_0'\right] = 0, \tag{31}$$
$$\left(\frac{1+N_R}{Pr}\right)\Theta_1'' + \Theta_1' + Df\Phi_1'' + He\Theta_0 = 0, \tag{32}$$
$$\frac{1}{Sc}\Phi_1'' + \Phi_1' + Sr\Theta_1'' - \delta\Phi_0 = 0, \tag{33}$$

subject to the boundary conditions:

$$\begin{aligned}
&F_1(\xi,0) = 0, \quad F_1'(\xi,0) = 0, \quad F_1'(\xi,\infty) = 0,\\
&G_1(\xi,0) = 0, \quad G_1(\xi,\infty) = 0,\\
&\Theta_1(\xi,0) = 0, \quad \Theta_1(\xi,\infty) = 0,\\
&\Phi_1(\xi,0) = 0, \quad \Phi_1(\xi,\infty) = 0.
\end{aligned} \tag{34}$$

The equations for $k \geq 2$ are obtained as:

$$F_k''' + F_k'' + \Theta_k = \frac{1}{2}\sum_{s=0}^{k-2}s\left(F_{k-2-s}''F_s - F_{k-2-s}'F_s'\right) + \frac{M}{1+m^2}\left[F_{k-1}' + mG_{k-1}\right], \tag{35}$$

$$G_k'' + G_k' = \frac{1}{2}\sum_{s=0}^{k-2}s\left(G_{k-2-s}'F_s - F_{k-2-s}'G_s\right) + \frac{M}{1+m^2}\left[G_{k-1} + mF_{k-1}'\right], \tag{36}$$

$$\left(\frac{1+N_R}{Pr}\right)\Theta_k'' + \Theta_k' + Df\Phi_k'' = \frac{1}{2}\sum_{s=0}^{k-2}s\left(\Theta_{k-2-s}'F_s - \sum_{s=0}^{k-2}F_{k-2-s}'\Theta_s\right) - He\Theta_{k-1}, \tag{37}$$

$$\frac{1}{Sc}\Phi_k'' + \Phi_k' + Sr\Theta_k'' = \frac{1}{2}\sum_{s=0}^{k-2}s\left(\Phi_{k-2-s}'F_s - \sum_{s=0}^{k-2}F_{k-2-s}'\Theta_s\right) + \delta\Phi_{k-1}, \tag{38}$$

subject to the following boundary conditions

$$\begin{aligned}
&F_k(\xi,0) = 0, \quad F_k'(\xi,0) = 0, \quad F_k'(\xi,\infty) = 0,\\
&G_k(\xi,0) = 0, \quad G_k(\xi,\infty) = 0,\\
&\Theta_k(\xi,0) = 0, \quad \Theta_k(\xi,\infty) = 0,\\
&\Phi_k(\xi,0) = 0, \quad \Phi_k(\xi,\infty) = 0.
\end{aligned} \tag{39}$$

The initial solution at $k = 0$ used to start the LSPM algorithm can be obtained by solving equations (25) - (28) subject to the boundary conditions (29). Also, the solution at $k = 1$ can be found by solving equations (30) - (33) subject to the boundary conditions (34). We remark that equations (25) -

(28) and equations (30) - (33) are interlinked and cannot be solved independently of each other or solved exactly and therefore must be solved numerically as a coupled system. The Chebyshev spectral collocation method is very accurate and convenient to use in solving differential equations of the type (25) - (28), (30) - (33) and (35) - (38) which are linear with constant coefficients. For brevity, details of the spectral method have been omitted in this paper. Interested readers can refer to the works of (see[15], [16], [17]) on how the spectral collocation method has been used to solve similar partial differential equations. Applying the spectral method on equations (25) - (28) gives:

$$\begin{bmatrix} \Delta_{1,1} & \Delta_{1,2} & \Delta_{1,3} & \Delta_{1,4} \\ \Delta_{2,1} & \Delta_{2,2} & \Delta_{2,3} & \Delta_{2,4} \\ \Delta_{3,1} & \Delta_{3,2} & \Delta_{3,3} & \Delta_{3,4} \\ \Delta_{4,1} & \Delta_{4,2} & \Delta_{4,3} & \Delta_{4,4} \end{bmatrix} \begin{bmatrix} \mathbf{F}_0 \\ \mathbf{G}_0 \\ \mathbf{\Theta}_0 \\ \mathbf{\Phi}_0 \end{bmatrix} = \begin{bmatrix} \mathbf{Z}_1 \\ \mathbf{Z}_2 \\ \mathbf{Z}_3 \\ \mathbf{Z}_4 \end{bmatrix}, \quad (40)$$

where

$$\begin{aligned}
&\Delta_{1,1} = \mathbf{D}^3 + \mathbf{D}^2, \quad \Delta_{1,2} = \mathbf{0}, \quad \Delta_{1,3} = \mathbf{I}, \quad \Delta_{1,4} = \mathbf{0}, \\
&\Delta_{2,1} = \mathbf{0}, \quad \Delta_{2,2} = \mathbf{D}^2 + \mathbf{D}, \quad \Delta_{2,3} = \mathbf{0}, \quad \Delta_{2,4} = \mathbf{0}, \\
&\Delta_{3,1} = \mathbf{0}, \quad \Delta_{3,2} = \mathbf{0}, \quad \Delta_{3,3} = \left(\frac{1 + N_R}{Pr}\right)\mathbf{D}^2 + \mathbf{D}, \\
&\Delta_{3,4} = (Df)\,\mathbf{D}^2, \quad \Delta_{4,1} = \mathbf{0}, \quad \Delta_{4,2} = \mathbf{0}, \quad \Delta_{4,3} = (Sr)\,\mathbf{D}^2, \\
&\Delta_{4,4} = \left(\frac{1}{Sc}\right)\mathbf{D}^2 + \mathbf{D}, \\
&\mathbf{Z}_1 = \mathbf{0}, \quad \mathbf{Z}_2 = \mathbf{0}, \quad ,\mathbf{Z}_3 = \mathbf{0}, \quad \mathbf{Z}_4 = \mathbf{0}, \qquad (41)
\end{aligned}$$

where $\mathbf{D} = 2D/L_\infty$, with D being the Chebyshev spectral differentiation matrix of size $(N_x + 1) \times (N_x + 1)$ whose entries are defined in [18], [19], L_∞ is a finite value selected to be large to approximate the conditions at infinity, $\mathbf{I}$ is an identity matrix of size $(N_x + 1) \times (N_x + 1)$ and $\mathbf{0}$ is a zero vector of size $(N_x+1)\times 1$. Also, applying spectral collocation method on equations (30) - (33) gives:

$$\begin{bmatrix} \Lambda_{1,1} & \Lambda_{1,2} & \Lambda_{1,3} & \Lambda_{1,4} \\ \Lambda_{2,1} & \Lambda_{2,2} & \Lambda_{2,3} & \Lambda_{2,4} \\ \Lambda_{3,1} & \Lambda_{3,2} & \Lambda_{3,3} & \Lambda_{3,4} \\ \Lambda_{4,1} & \Lambda_{4,2} & \Lambda_{4,3} & \Lambda_{4,4} \end{bmatrix} \begin{bmatrix} \mathbf{F}_1 \\ \mathbf{G}_1 \\ \mathbf{\Theta}_1 \\ \mathbf{\Phi}_1 \end{bmatrix} = \begin{bmatrix} \mathbf{R}_1 \\ \mathbf{R}_2 \\ \mathbf{R}_3 \\ \mathbf{R}_4 \end{bmatrix}, \quad (42)$$

where

$$\begin{aligned}
&\Lambda_{1,1} = \mathbf{D}^3 + \mathbf{D}^2, \quad \Lambda_{1,2} = \mathbf{0}, \quad \Lambda_{1,3} = \mathbf{I}, \quad \Lambda_{1,4} = \mathbf{0}, \\
&\Lambda_{2,1} = \mathbf{0}, \quad \Lambda_{2,2} = \mathbf{D}^2 + \mathbf{D}, \quad \Lambda_{2,3} = \mathbf{0}, \quad \Lambda_{2,4} = \mathbf{0}, \\
&\Lambda_{3,1} = \mathbf{0}, \quad \Lambda_{3,2} = \mathbf{0}, \quad \Lambda_{3,3} = \left(\frac{1 + N_R}{Pr}\right)\mathbf{D}^2 + \mathbf{D} + (He)\,\mathbf{I}, \\
&\Lambda_{3,4} = (Df)\,\mathbf{D}^2, \quad \Lambda_{4,1} = \mathbf{0}, \quad \Lambda_{4,2} = \mathbf{0}, \quad \Lambda_{4,3} = (Sr)\,\mathbf{D}^2, \\
&\Lambda_{4,4} = \left(\frac{1}{Sc}\right)\mathbf{D}^2 + \mathbf{D} - (\delta)\,\mathbf{I}, \\
&\mathbf{R}_1 = \left(\frac{M}{1+m^2}\right)(\mathbf{F}_0)\,\mathbf{D} + \left(\frac{M}{1+m^2}m\right)\mathbf{G}_0, \\
&\mathbf{R}_2 = \left(\frac{M}{1+m^2}\right)\mathbf{G}_0 - \left(\frac{M}{1+m^2}m\right)(\mathbf{F}_0)\,\mathbf{D}, \\
&\mathbf{R}_3 = -(He)\,\mathbf{\Theta}_0, \quad \mathbf{R}_4 = \delta\mathbf{\Phi}_0. \qquad (43)
\end{aligned}$$

Solutions to the higher order approximations F_k, G_k, Θ_k and Φ_k for $k \geq 2$ given by equations (35) - (38) can then be obtained using the spectral method. It is for this reason the method is refereed to as the large parameter spectral perturbation method. Similarly, applying the spectral collocation method on equations (35) - (38) gives:

$$\begin{bmatrix} \mathbf{A}_{1,1} & \mathbf{A}_{1,2} & \mathbf{A}_{1,3} & \mathbf{A}_{1,4} \\ \mathbf{A}_{2,1} & \mathbf{A}_{2,2} & \mathbf{A}_{2,3} & \mathbf{A}_{2,4} \\ \mathbf{A}_{3,1} & \mathbf{A}_{3,2} & \mathbf{A}_{3,3} & \mathbf{A}_{3,4} \\ \mathbf{A}_{4,1} & \mathbf{A}_{4,2} & \mathbf{A}_{4,3} & \mathbf{A}_{4,4} \end{bmatrix} \begin{bmatrix} \mathbf{F}_k \\ \mathbf{G}_k \\ \mathbf{\Theta}_k \\ \mathbf{\Phi}_k \end{bmatrix} = \begin{bmatrix} \mathbf{Q}_{1,k-2} \\ \mathbf{Q}_{2,k-2} \\ \mathbf{Q}_{3,k-2} \\ \mathbf{Q}_{4,k-2} \end{bmatrix}, \quad (44)$$

where

$$\begin{aligned}
&\mathbf{A}_{1,1} = \mathbf{D}^3 + \mathbf{D}^2, \quad \mathbf{A}_{1,2} = \mathbf{0}, \quad \mathbf{A}_{1,3} = \mathbf{I}, \quad \mathbf{A}_{1,4} = \mathbf{0}, \\
&\mathbf{A}_{2,1} = \mathbf{0}, \quad \mathbf{A}_{2,2} = \mathbf{D}^2 + \mathbf{D}, \quad \mathbf{A}_{2,3} = \mathbf{0}, \quad \mathbf{A}_{2,4} = \mathbf{0}, \\
&\mathbf{A}_{3,1} = \mathbf{0}, \quad \mathbf{A}_{3,2} = \mathbf{0}, \quad \mathbf{A}_{3,3} = \left(\frac{1 + N_R}{Pr}\right)\mathbf{D}^2 + \mathbf{D} + (He)\,\mathbf{I}, \\
&\mathbf{A}_{3,4} = (Df)\,\mathbf{D}^2, \quad \mathbf{A}_{4,1} = \mathbf{0}, \quad \mathbf{A}_{4,2} = \mathbf{0}, \quad \mathbf{A}_{4,3} = (Sr)\,\mathbf{D}^2, \\
&\mathbf{A}_{4,4} = \left(\frac{1}{Sc}\right)\mathbf{D}^2 + \mathbf{D} - (\delta)\,\mathbf{I}, \\
&\mathbf{Q}_{1,k-2} = \mathrm{Sum}\mathbf{F} + \left(\frac{M}{1+m^2}\right)(\mathbf{D}\mathbf{F}_{k-1}) + \left(\frac{M}{1+m^2}m\right)\mathbf{G}_{k-1}, \\
&\mathbf{Q}_{2,k-2} = \mathrm{Sum}\mathbf{G} + \left(\frac{M}{1+m^2}\right)\mathbf{G}_{k-1} - \left(\frac{M}{1+m^2}m\right)(\mathbf{D}\mathbf{F}_{k-1}), \\
&\mathbf{Q}_{3,k-2} = \mathrm{Sum}\mathbf{\Theta} - (He)\,\mathbf{\Theta}_{k-1}, \\
&\mathbf{Q}_{4,k-2} = \mathrm{Sum}\mathbf{\Phi} + \delta\mathbf{\Phi}_{k-1}, \qquad (45)
\end{aligned}$$

where $\mathrm{Sum}\mathbf{F}$, $\mathrm{Sum}\mathbf{G}$, $\mathrm{Sum}\mathbf{\Theta}$ and $\mathrm{Sum}\mathbf{\Phi}$ are defined as:

$$\begin{aligned}
\mathrm{Sum}\mathbf{F} &= \frac{1}{2}\sum_{s=0}^{k-2}\left(\mathbf{D}^2\mathbf{F}_{k-2-s}\right)(s\mathbf{F}_s) - \frac{1}{2}\sum_{s=0}^{k-2}\left(\mathbf{D}\mathbf{F}_{k-2-s}\right)(s\mathbf{D}\mathbf{F}_s), \\
\mathrm{Sum}\mathbf{G} &= \frac{1}{2}\sum_{s=0}^{k-2}\left(\mathbf{D}\mathbf{G}_{k-2-s}\right)(s\mathbf{F}_s) - \frac{1}{2}\sum_{s=0}^{k-2}\left(\mathbf{D}\mathbf{F}_{k-2-s}\right)(s\mathbf{G}_s), \\
\mathrm{Sum}\mathbf{\Theta} &= \frac{1}{2}\sum_{s=0}^{k-2}\left(\mathbf{D}\mathbf{\Theta}_{k-2-s}\right)(s\mathbf{F}_s) - \frac{1}{2}\sum_{s=0}^{k-2}\left(\mathbf{D}\mathbf{F}_{k-2-s}\right)(s\mathbf{\Theta}_s), \\
\mathrm{Sum}\mathbf{\Phi} &= \frac{1}{2}\sum_{s=0}^{k-2}\left(\mathbf{D}\mathbf{\Phi}_{k-2-s}\right)(s\mathbf{F}_s) - \frac{1}{2}\sum_{s=0}^{m-1}\left(\mathbf{D}\mathbf{F}_{k-2-s}\right)(s\mathbf{\Phi}_s).
\end{aligned}$$

Therefore, starting from the known $\mathbf{F}_0$, $\mathbf{G}_0$, $\mathbf{\Theta}_0$, $\mathbf{\Phi}_0$, $\mathbf{F}_1$, $\mathbf{G}_1$, $\mathbf{\Theta}_1$, and $\mathbf{\Phi}_1$ the solutions are obtained as:

$$\mathbf{V}_m = \mathbf{A}^{-1}\mathbf{Q}_{i,k-2}, \quad (46)$$

where

$$\mathbf{A} = \begin{bmatrix} \mathbf{A}_{1,1} & \mathbf{A}_{1,2} & \mathbf{A}_{1,3} & \mathbf{A}_{1,4} \\ \mathbf{A}_{2,1} & \mathbf{A}_{2,2} & \mathbf{A}_{2,3} & \mathbf{A}_{2,4} \\ \mathbf{A}_{3,1} & \mathbf{A}_{3,2} & \mathbf{A}_{3,3} & \mathbf{A}_{3,4} \\ \mathbf{A}_{4,1} & \mathbf{A}_{4,2} & \mathbf{A}_{4,3} & \mathbf{A}_{4,4} \end{bmatrix}, \quad \mathbf{V}_k = \begin{bmatrix} \mathbf{F}_k \\ \mathbf{G}_k \\ \mathbf{\Theta}_k \\ \mathbf{\Phi}_k \end{bmatrix},$$

$$\mathbf{Q}_{i,k-2} = \begin{bmatrix} \mathbf{Q}_{1,k-2} \\ \mathbf{Q}_{2,k-2} \\ \mathbf{Q}_{3,k-2} \\ \mathbf{Q}_{4,k-2} \end{bmatrix}.$$

IV. Results and discussion

In this section, numerical solutions of the governing system of nonlinear partial differential equations (11) - (14), subject to the boundary conditions (15) obtained using the large parameter spectral perturbation method (LSPM) are presented. To verify the accuracy of the LSPM, the present numerical results are confirmed against the multi-domain bivariate spectral quasilinearisation method (MD-BSQLM). We remark that the multi-domain approach was applied only in the ξ direction. We further present the convergence of the series solutions, residual error, the significance of the system parameters on the fluid properties, the variation of the local skin-friction coefficient, Nusselt number and Sherwood number with different flow parameters. From our numerical simulations it was observed that $N_x = 100$ collocation points in the space variable η and $N_t = 5$ collocation points for the transpiration parameter ξ were sufficient to give accurate results in all the spectral method discretization done. Furthermore, the finite value selected to be largely used to the boundary condition at infinity was set to be $L_\infty = 40$ in the LSPM and $L_\infty = 10$ in the MD-BSQLM, if not stated.

Table I gives the LSPM numerical values of the local skin-friction $C_{fx}Gr_x^{-3/4}$, and local Nusselt number $Nu_xGr_x^{-1/4}$ for various values of the transpiration parameter ξ, and a comparison with the MD-BSQLM numerical results and results of Saha et al. [7] in the absence of mass, Soret, Dufour, thermal radiation, heat generation and chemical reaction parameters. A good agreement is achieved. From the table, we observe that as there is an increase in the value of the transpiration parameter the local skin-friction decreases while the local Nusselt number increases. Table II shows the computed values of the local skin-friction coefficient, $C_{fx}Gr_x^{-3/4}$, local Nusselt number $Nu_xGr_x^{-1/4}$ and local Sherwood number $Sh_xGr_x^{-1/4}$ for different values of Dufour Df, and Soret Sr parameters. It is noticed from the table that a good agreement between the LSPM and the MD-BSQLM numerical solutions is observed. The table also gives the order of LSPM series approximation k required to obtain accurate results that are comparable with the MD-BSQLM and are consistent up to six decimal places. It can be seen from the table that more than one, two, or three of the series terms or approximation is required to obtain the results displayed in the table. This corroborates the fact, that it is expedient to obtain higher order series approximation in order to get accurate results.

Tables (III) - (VI) presents the variation of the solution error of the approximate numerical solutions of $F(0,\xi)$, $G(0,\xi)$ $\Theta(0,\xi)$ and $\Phi(0,\xi)$ against increasing order (k) of the LSPM series approximation for different values of ξ. We observe the error reduces as the order of series approximation increases. Also as ξ becomes larger, the error becomes smaller, this is because the series expansion was done inversely proportional to ξ. This suggests that the method is convergent. The success of the method is linked to the fact that series expansion was done inversely about a large parameter and the Chebyshev spectral collocation method was used to solve the higher order perturbation equations in the space direction.

The accuracy of the LSPM is confirmed by using the solution error of the functions after a specified number of series approximation. The solution error of the functions are defined as:

$$\begin{aligned}
E_F &= ||\mathbf{F}_{k+1} - \mathbf{F}_k||_\infty,\\
E_G &= ||\mathbf{G}_{k+1} - \mathbf{G}_k||_\infty,\\
E_\Theta &= ||\mathbf{\Theta}_{k+1} - \mathbf{\Theta}_k||_\infty,\\
E_\Phi &= ||\mathbf{\Phi}_{k+1} - \mathbf{\Phi}_k||_\infty. \qquad (47)
\end{aligned}$$

The errors defined by equation (47) are considered as the solution based error where $k+1$, and k represents the solution with the first $k+1$, k terms of the series approximation, respectively. We remark that if the iterative scheme is converging, the errors are expected to decrease with an increase in the order of series approximation. In order to further establish the accuracy of the LSPM numerical method, we have also considered the residual error which is a representation of the extent at which the solution of the governing partial differential equations (19) - (22) is approximated by the numerical solution. We substitute the approximate solutions into equations (19) - (22) and determine the maximum norm of the residual error. Accordingly, we define the maximum error of the residual as:

$$\begin{aligned}
Res(F) &= \max_{0\le j\le N_x} |\bar{N}_F\left[\mathbf{F}_k(\xi,\eta), \mathbf{G}_k(\xi,\eta), \mathbf{\Theta}_k(\xi,\eta)\right]|,\\
Res(G) &= \max_{0\le j\le N_x} |\bar{N}_G\left[\mathbf{F}_k(\xi,\eta), \mathbf{G}_k(\xi,\eta)\right]|,\\
Res(\Theta) &= \max_{0\le j\le N_x} |\bar{N}_\Theta\left[\mathbf{F}_k(\xi,\eta), \mathbf{\Theta}_k(\xi,\eta), \mathbf{\Phi}_k(\xi,\eta)\right]|,\\
Res(\Phi) &= \max_{0\le j\le N_x} |\bar{N}_\Phi\left[\mathbf{F}_k(\xi,\eta), \mathbf{\Theta}_k(\xi,\eta), \mathbf{\Phi}_k(\xi,\eta)\right]|, \qquad (48)
\end{aligned}$$

where $\bar{N}_F, \bar{N}_G$, $\bar{N}_\Theta$ and $\bar{N}_\Phi$ are the governing nonlinear partial differential equations defined as:

$$\begin{aligned}
\bar{N}_F &= F''' + F'' + \Theta - \frac{M}{1+m^2}\xi^{-2}\left[F' + mG\right]\\
&\quad - \frac{1}{4}\xi^{-3}\left[F'\frac{\partial F'}{\partial \xi} - F''\frac{\partial F}{\partial \xi}\right],\\
\bar{N}_G &= G'' + G' - \frac{M}{1+m^2}\xi^{-2}\left[G - mF'\right]\\
&\quad - \frac{1}{4}\xi^{-3}\left[F'\frac{\partial G}{\partial \xi} - G'\frac{\partial F}{\partial \xi}\right],\\
\bar{N}_\Theta &= \left(\frac{1+N_R}{Pr}\right)\Theta'' + \Theta' + \xi^{-2}He\Theta + Df\Phi''\\
&\quad - \frac{1}{4}\xi^{-3}\left[F'\frac{\partial \Theta}{\partial \xi} - \Theta'\frac{\partial F}{\partial \xi}\right],\\
\bar{N}_\Phi &= \frac{1}{Sc}\Phi'' + \Phi' - \xi^{-2}\delta\Phi + Sr\Theta'' - \frac{1}{4}\xi^{-3}\left[F'\frac{\partial \Phi}{\partial \xi} - \Phi'\frac{\partial F}{\partial \xi}\right],
\end{aligned}$$

and $\mathbf{F}_k(\xi,\eta), \mathbf{G}_k(\xi,\eta), \mathbf{\Theta}_k(\xi,\eta)$, and$\mathbf{\Phi}_k(\xi,\eta)$ are the LSPM approximate solutions.

Figures 2 - 4 shows the tangential velocity, temperature and transverse velocity profiles for the transpiration parameter ξ. The velocity and temperature profiles are reduced for higher transpiration parameter values suggesting that as the transpiration parameter increases, there is a decrease in the fluid velocity and temperature. This is due to the suction effects of the surface mass transfer. A similar trend for the tangential velocity and temperature profiles was observed in the study carried out by Saha et al. [7].

Figures 5 and 6 shows the effect of magnetic parameter M on the tangential and transverse velocity profiles. We note from the Figures that the tangential velocity diminishes while the transverse velocity enhances. The flow pattern observation recorded in Figure 5 is so because the magnetic field acts as an opposing or resistive force on the fluid. Further, the magnetic field has the tendency to slow down the motion of the fluid. The variation of the Hall parameter m on the tangential velocity and transverse velocity profiles are displayed in Figures 7 and 8. We observe from Figure 7 that the tangential velocity profile is increased for higher values m, while, in Figure 5, it can be seen from the graph that there is a decrease in the transverse velocity profile when increasing the Hall parameter.

We show the effect of the Dufour number Df on the temperature profile in Figure 9. We observe an enhancement of the temperature profile in Figure 9 as the Dufour number is increased. We remark that there is always a gradual decay of the temperature profile when the ratio between the temperature and concentration gradient is very small.

The effect of heat generation parameter He is shown in Figure 10. We observe here, as would be expected, that the temperature profile is enhanced by increasing heat generation for the shear thinning and shear thickening fluids. In physical terms, the heat generation parameter increases fluid temperature, and thus leads to an increase in the thermal boundary layer thickness.

TABLE I
COMPARISON OF THE LSPM AND MD-BSQLM APPROXIMATE NUMERICAL SOLUTIONS RESULT FOR LOCAL SKIN FRICTION $C_{fx}Gr_x^{-3/4}$ AND LOCAL NUSSELT NUMBER $Nu_xGr_x^{-1/4}$ AGAINST THOSE EXISTING IN LITERATURE FOR VARIOUS VALUES OF ξ WHEN $Pr = 0.7$, $M = 0.5$, $m = 100$, $Sc = Sr = N_R = \delta = 0$ AND $He = 0$.

ξ	$C_{fx}Gr_x^{-3/4}$			$Nu_xGr_x^{-1/4}$		
	LSPM	MD-BSQLM	[7]	LSPM	MD-BSQLM	[7]
2.00	0.7084	0.7090	0.7086	1.4030	1.4027	1.4050
2.50	0.5714	0.5714	0.5717	1.7500	1.7500	1.7499
5.00	0.2857	0.2857	0.2857	3.5000	3.5000	3.5000
20.00	0.0714	0.0714	0.0714	14.0000	14.0000	14.0000
40.00	0.0357	0.0357	0.0357	28.0000	28.0000	28.0000
50.00	0.0286	0.0286	0.0286	35.0000	35.0000	35.0000
60.00	0.0238	0.0238	0.0238	42.0000	42.0000	42.0000
70.00	0.0204	0.0204	0.0204	49.0000	49.0000	49.0000
80.00	0.0179	0.0179	0.0179	56.0000	56.0000	56.0000

TABLE II
TABLE OF VALUES OF LOCAL SKIN-FRICTION COEFFICIENT, LOCAL NUSSELT NUMBER, COMPARISON OF THE LSPM AND MD-BSQLM APPROXIMATE NUMERICAL SOLUTIONS RESULT FOR LOCAL SKIN FRICTION $C_{fx}Gr_x^{-3/4}$, LOCAL NUSSELT NUMBER $Nu_xGr_x^{-1/4}$ AND LOCAL SHERWOOD NUMBER $Sh_xGr_x^{-1/4}$ AGAINST MD-BSQLM NUMERICAL RESULTS FOR VARIOUS VALUES OF DUFOUR NUMBER Df AND SORET NUMBER Sr WHEN $\xi = 5$, $Pr = 0.7$, $M = 0.5$, $m = 100$, $Sc = 1$, $He = 0.2$, $\delta = 1$, AND $N_R = 0.2$.

Df	Sr	$C_{fx}Gr_x^{-3/4}$			$Nu_xGr_x^{-1/4}$			$Sh_xGr_x^{-1/4}$		
		LSPM	k	MD-BSQLM	LSPM	k	MD-BSQLM	LSPM	k	MD-BSQLM
0.1	0.2	0.368198	6	0.368198	2.598939	8	2.598939	4.708836	8	4.708836
	0.3	0.368213	6	0.368213	2.613299	6	2.613299	4.462631	7	4.462631
	0.4	0.368228	6	0.368228	2.627831	6	2.627831	4.213487	8	4.213487
	0.5	0.368243	6	0.368243	2.642537	6	2.642537	3.961349	8	3.961349
	0.6	0.368258	6	0.368258	2.657421	6	2.657421	3.706164	8	3.706164
0.2	0.2	0.388675	6	0.388675	2.315250	6	2.315250	4.765445	8	4.765445
	0.3	0.388706	7	0.388706	2.341068	8	2.341068	4.544106	8	4.544106
	0.4	0.388736	6	0.388736	2.367519	6	2.367519	4.317352	8	4.317352
	0.5	0.388766	6	0.388766	2.394625	6	2.394625	4.084980	9	4.084980
	0.6	0.388796	6	0.388796	2.422411	7	2.422411	3.846781	8	3.846781
0.4	0.2	0.429630	6	0.429630	1.727084	6	1.727084	4.882821	8	4.882821
	0.3	0.429690	6	0.429690	1.765941	7	1.765941	4.716256	8	4.716256
	0.4	0.429750	6	0.429750	1.806797	8	1.806797	4.541122	8	4.541122
	0.5	0.429810	6	0.429810	1.849812	8	1.849812	4.356739	8	4.356739
	0.6	0.429870	7	0.429870	1.895161	7	1.895161	4.162354	9	4.162354
0.5	0.2	0.450108	7	0.450108	1.422093	7	1.422093	4.943690	9	4.943690
	0.3	0.450182	6	0.450182	1.461868	7	1.461868	4.807284	8	4.807284
	0.4	0.450257	6	0.450257	1.504269	8	1.504269	4.661874	9	4.661874
	0.5	0.450332	8	0.450332	1.549565	8	1.549565	4.506539	8	4.506539
	0.6	0.450406	6	0.450406	1.598064	8	1.598064	4.340225	10	4.340225
0.6	0.2	0.470584	6	0.470584	1.109465	7	1.109465	5.006088	8	5.006088
	0.3	0.470675	7	0.470675	1.145928	7	1.145928	4.901873	8	4.901873
	0.4	0.470764	7	0.470764	1.185358	8	1.185358	4.789180	8	4.789180
	0.5	0.470853	7	0.470853	1.228133	8	1.228133	4.666932	8	4.666932
	0.6	0.470942	7	0.470942	1.274698	8	1.274698	4.533857	8	4.533857

TABLE III
SOLUTION ERROR OF $F(0,\xi)$ WITH INCREASE IN ORDER OF LSPM APPROXIMATION WHEN $Pr = 0.7$, $M = 0.5$, $m = 100$, $Sc = 1$, $He = 0.2$, $\delta = 1$, AND $N_R = 0.2$.

$k \setminus \xi$	5	10	15	20	25	30	40
1	7.28×10^{-5}	1.82×10^{-5}	8.09×10^{-6}	4.55×10^{-6}	2.91×10^{-6}	2.02×10^{-6}	1.14×10^{-6}
2	2.31×10^{-7}	1.44×10^{-8}	2.85×10^{-9}	9.02×10^{-10}	3.70×10^{-10}	1.78×10^{-11}	5.64×10^{-12}
3	2.21×10^{-9}	3.45×10^{-11}	3.03×10^{-12}	5.40×10^{-13}	9.95×10^{-14}	4.74×10^{-15}	8.43×10^{-16}
4	1.11×10^{-11}	4.34×10^{-14}	1.69×10^{-15}	1.70×10^{-16}	2.84×10^{-17}	6.61×10^{-18}	6.62×10^{-19}
5	9.53×10^{-14}	9.31×10^{-17}	1.61×10^{-18}	9.09×10^{-20}	9.76×10^{-21}	1.58×10^{-21}	8.88×10^{-23}
6	4.22×10^{-16}	1.03×10^{-19}	7.95×10^{-22}	2.52×10^{-23}	1.73×10^{-24}	1.94×10^{-25}	6.15×10^{-27}
7	3.12×10^{-18}	1.91×10^{-22}	6.53×10^{-25}	1.16×10^{-26}	5.11×10^{-28}	3.98×10^{-29}	7.10×10^{-31}
8	2.31×10^{-21}	3.56×10^{-26}	5.42×10^{-29}	5.44×10^{-31}	1.53×10^{-32}	8.28×10^{-34}	8.30×10^{-36}
9	7.87×10^{-23}	3.00×10^{-28}	2.03×10^{-31}	1.14×10^{-33}	2.06×10^{-35}	7.75×10^{-37}	4.37×10^{-39}
10	3.15×10^{-24}	3.01×10^{-30}	9.04×10^{-34}	2.87×10^{-36}	3.31×10^{-38}	8.63×10^{-40}	2.74×10^{-42}

The effect of radiation parameter N_R on the temperature profile is displayed in Figure 11. We note from the figure that an increase in the radiation parameter results in an increasing temperature profile within the boundary layer. This is due to an increase in thermal boundary layer thickness.

Figure 12 illustrates the effect of the Prandtl number Pr on the temperature profile. The temperature profile, as well as the thermal boundary layer thickness, diminishes with increasing Pr. The effect is more pronounced with smaller values of Pr because smaller values of Pr increases the thermal conductivity of the fluid and hence heat diffuses away more rapidly from the heated surface than for higher values of Pr.

Figures 13 represent the concentration profile for different

TABLE IV
SOLUTION ERROR OF $G(0,\xi)$ WITH INCREASE IN ORDER OF LSPM APPROXIMATION WHEN $Pr = 0.7$, $M = 0.5$, $m = 100$, $Sc = 1$, $He = 0.2$, $\delta = 1$, AND $N_R = 0.2$.

$k \setminus \xi$	5	10	15	20	25	30	40
1	1.14×10^{-6}	2.84×10^{-7}	1.26×10^{-7}	7.10×10^{-8}	4.51×10^{-8}	3.15×10^{-8}	1.77×10^{-9}
2	2.27×10^{-9}	1.42×10^{-10}	2.80×10^{-11}	8.85×10^{-12}	3.62×10^{-12}	1.75×10^{-13}	5.53×10^{-14}
3	2.78×10^{-12}	4.35×10^{-14}	3.82×10^{-15}	6.79×10^{-16}	1.78×10^{-16}	5.96×10^{-17}	1.06×10^{-18}
4	1.01×10^{-13}	3.93×10^{-16}	1.53×10^{-17}	1.54×10^{-18}	2.58×10^{-19}	5.99×10^{-20}	6.00×10^{-21}
5	3.95×10^{-16}	3.86×10^{-19}	6.69×10^{-21}	3.77×10^{-22}	4.05×10^{-23}	6.54×10^{-24}	3.68×10^{-25}
6	5.03×10^{-18}	1.23×10^{-21}	9.46×10^{-24}	3.00×10^{-25}	2.06×10^{-26}	2.31×10^{-27}	7.32×10^{-29}
7	1.96×10^{-20}	1.20×10^{-24}	4.10×10^{-27}	7.30×10^{-29}	3.21×10^{-30}	2.50×10^{-31}	4.45×10^{-33}
8	2.16×10^{-22}	3.30×10^{-27}	5.02×10^{-30}	5.03×10^{-32}	1.42×10^{-33}	7.66×10^{-35}	7.68×10^{-37}
9	1.16×10^{-25}	4.44×10^{-31}	3.00×10^{-34}	1.69×10^{-36}	3.05×10^{-38}	1.15×10^{-39}	6.46×10^{-42}
10	2.11×10^{-27}	2.01×10^{-33}	6.05×10^{-37}	1.92×10^{-39}	2.21×10^{-41}	5.77×10^{-43}	1.83×10^{-45}

TABLE V
SOLUTION ERROR OF $\Theta(0,\xi)$ WITH INCREASE IN ORDER OF LSPM APPROXIMATION WHEN $Pr = 0.7$, $M = 0.5$, $m = 100$, $Sc = 1$, $He = 0.2$, $\delta = 1$, AND $N_R = 0.2$.

$k \setminus \xi$	5	10	15	20	25	30	40
1	1.23×10^{-3}	3.08×10^{-4}	1.37×10^{-4}	7.71×10^{-5}	4.93×10^{-5}	3.43×10^{-5}	1.93×10^{-6}
2	3.87×10^{-6}	2.42×10^{-7}	4.77×10^{-8}	1.51×10^{-8}	6.19×10^{-9}	2.98×10^{-9}	9.44×10^{-10}
3	2.83×10^{-8}	4.42×10^{-10}	3.88×10^{-11}	6.91×10^{-12}	1.81×10^{-13}	6.07×10^{-14}	1.08×10^{-15}
4	1.50×10^{-10}	5.87×10^{-13}	2.29×10^{-14}	2.65×10^{-15}	3.85×10^{-16}	8.95×10^{-17}	8.96×10^{-18}
5	1.01×10^{-12}	9.85×10^{-16}	1.71×10^{-17}	9.62×10^{-19}	1.03×10^{-20}	1.67×10^{-21}	9.39×10^{-22}
6	4.66×10^{-15}	1.14×10^{-18}	8.77×10^{-21}	2.78×10^{-22}	1.91×10^{-23}	2.14×10^{-24}	6.78×10^{-26}
7	2.20×10^{-17}	1.34×10^{-21}	4.59×10^{-24}	8.18×10^{-26}	3.60×10^{-27}	2.80×10^{-28}	4.99×10^{-30}
8	1.23×10^{-19}	1.87×10^{-24}	2.85×10^{-27}	2.86×10^{-29}	8.05×10^{-31}	4.35×10^{-32}	4.36×10^{-34}
9	2.01×10^{-21}	7.67×10^{-27}	5.19×10^{-30}	2.93×10^{-32}	5.27×10^{-34}	1.98×10^{-35}	1.12×10^{-37}
10	3.45×10^{-23}	3.29×10^{-29}	9.89×10^{-33}	3.14×10^{-35}	3.62×10^{-37}	9.43×10^{-39}	2.99×10^{-41}

TABLE VI
SOLUTION ERROR OF $\Phi(0,\xi)$ WITH INCREASE IN ORDER OF LSPM APPROXIMATION WHEN $Pr = 0.7$, $M = 0.5$, $m = 100$, $Sc = 1$, $He = 0.2$, $\delta = 1$, AND $N_R = 0.2$.

$k \setminus \xi$	5	10	15	20	25	30	40
1	2.79×10^{-3}	6.99×10^{-4}	3.11×10^{-4}	1.75×10^{-4}	1.12×10^{-4}	7.76×10^{-5}	4.37×10^{-6}
2	1.28×10^{-5}	7.99×10^{-7}	1.58×10^{-7}	4.99×10^{-8}	2.04×10^{-8}	9.86×10^{-9}	3.12×10^{-10}
3	7.30×10^{-8}	1.14×10^{-9}	1.00×10^{-10}	1.78×10^{-11}	4.67×10^{-12}	1.57×10^{-13}	2.79×10^{-14}
4	4.10×10^{-10}	1.60×10^{-12}	3.36×10^{-14}	6.26×10^{-15}	1.05×10^{-16}	2.44×10^{-17}	2.44×10^{-18}
5	2.29×10^{-12}	2.23×10^{-15}	3.87×10^{-17}	2.18×10^{-18}	2.34×10^{-19}	3.78×10^{-20}	2.13×10^{-21}
6	1.07×10^{-14}	2.62×10^{-18}	2.02×10^{-20}	6.39×10^{-22}	4.39×10^{-23}	4.92×10^{-24}	1.56×10^{-25}
7	3.20×10^{-17}	1.96×10^{-21}	6.70×10^{-24}	1.19×10^{-25}	5.25×10^{-27}	4.09×10^{-28}	7.29×10^{-30}
8	3.98×10^{-19}	6.07×10^{-24}	9.25×10^{-27}	9.27×10^{-29}	2.61×10^{-30}	1.41×10^{-31}	1.41×10^{-33}
9	6.46×10^{-21}	2.47×10^{-26}	1.67×10^{-29}	9.41×10^{-29}	1.69×10^{-33}	6.36×10^{-35}	3.59×10^{-37}
10	7.89×10^{-23}	7.53×10^{-29}	2.26×10^{-32}	7.18×10^{-35}	8.28×10^{-37}	2.16×10^{-38}	6.85×10^{-41}

values of Soret number Sr. We observe from the figure that the concentration profile increase with the increasing values of Sr. This is beacause the mass flux produced by the temperature gradient increases the concentration profile.

In Figure 14, the effect of the chemical reaction parameter δ on the concentration profile is given. It is noticed that there is a decrease in the concentration profile when increasing the chemical reaction parameter. Physically, this implies that for a higher chemical reaction, there is a decrease in the chemical molecular diffusivity, leading to a reduction in mass diffusion, a decrease in the concentration of the diffusing species, which in turn leads to a thinning of the concentration boundary layer.

Figure 15 is drawn for concentration profile for different values of the Schmidt number Sc. We noticed from this figure that the effect of Schmidt number Sc is to decrease the concentration profile for lower values of Sc in the solutal boundary layer. As should be expected, the mass transfer rate decreases as Sc increases, that is, a decrease in the Schmidt number Sc decreases the concentration boundary layer thickness, which is attributed with the reduction in the concentration profile. Physically, the increase of Sc implies a decrease of molecular diffusion. Therefore, the concentration of the species is higher for large values of Sc and lower for small values of Sc.

The effect of magnetic parameter M on the local skin-friction $C_{fx}Gr_x^{-3/4}$ against the transpiration parameter ξ, is analyzed in Figure 16. It is observed that the local skin-friction decreases when the magnetic parameter increases. It is expected to have such observation because the amount of magnetic field inside the boundary layer enhances the Lorenz force that opposes the flow significantly in the reverse direction. Hence, the magnetic field serves as a retarding force that significantly decreases the coefficient of the local skin-friction.

Figure 17 depicts the effect of Hall parameter m on the local skin-friction $C_{fx}Gr_x^{-3/4}$ against the transpiration parameter ξ. From the figure, it is noted that the local skin-friction is enhanced by increasing the hall parameter. The Hall parameter is seen to support the fluid flow inside the boundary and thereby causing a rise in the skin-friction.

Figure 18 illustrates the effect of Dufour number Df on the local Nusselt number $Nu_xGr_x^{-1/4}$. It is observed that there is a decrease in the local Nusselt number when increasing the Dufour number.

Figure 19 display the effect of Soret number Sr on the local Sherwood number $Sh_x Gr_x^{-1/4}$. We observe from Figure 19 that an increase in the values of Soret number leads to a decrease in the Sherwood number.

Figures 20 - 23 are plotted to show the solution error of F, G, Θ and Φ against increasing order of the LSPM series approximation for different values of transpiration parameter ξ. The errors are known to be the difference between approximate values of the functions at two successive order of series approximation. The decrease in the solution error as the order of approximation increases is an indication that the numerical scheme converges. It can be seen that the error appears to be very small after ten order of approximation. This is because the series expansion was done inversely proportional to ξ. This observation correlate with earlier observation made in III - VI.

V. Conclusion

We have investigated MHD laminar convection flow from a vertical permeable flat plate with uniform surface temperature, Soret, Dufour, chemical reaction and thermal radiation. The transformed equations gave rise to coupled nonlinear partial differential equations. We have generated approximate numerical solutions of the coupled nonlinear system of partial differential equations using a large parameter spectral perturbation method. The study particularly aims at demonstrating that the large parameter spectral perturbation method can be used as a numerical tool for solving fluid mechanics problems related to the one considered in this investigation which has the Soret and Dufour effects and cannot be solved exactly even with methods that look for series solutions. Furthermore, numerical simulations were carried out to show the effects of the pertinent flow parameters on the flow model. The fluid temperature was found to increase with Dufour number while the local Nusselt number decreases with an increase in the values of Dufour number. The heat generation and thermal radiation parameter were found to increase both the temperature and thermal boundary layer thickness. The Soret number was reported to increase the fluid concentration while a reverse effect was observed on local Sherwood number with the increase in Soret number. In addition, the fluid concentration decreases with both the chemical reaction parameter and Schmidt numbers. Other flow parameter analysis were seen to be in agreement with those reported in the literature. Again, numerical computations were performed to show the convergence and accuracy of the LSPM. It was observed that the accuracy of the method improves as ξ becomes larger and as the order of series approximation increase with the residual and solution errors tending towards zero. The results from this investigation show that the LSPM is accurate, converges faster, easy to use and also gives accurate results valid for large values of the transpiration parameter ξ. The LSPM numerical method validation was confirmed by comparing with the multi-domain bivariate spectral quasilinearization method and a good agreement was achieved between the two sets of results. The LSPM and MD-BSQLM approximate numerical solutions were also found to be in agreement with those existing in the literature. The methods used in this study turned out to be successful thereby making it a reliable numerical tool for solving coupled nonlinear system of coupled partial differential equations similar to the one investigated in this study.

Acknowledgment

This work is based on the research supported wholly by the National Research Foundation of South Africa, the University of KwaZulu-Natal, South Africa, and Durban University of Technology, South Africa (Grant number: 116661).

References

[1] T. Yamanishi, "Hall effect of viscous flow of ionized gas through straight channels," *17th Annual Meeting, Physics Society of Japan*, vol. 5, pp. 29, 1962.

[2] K. R. Sing, and T. G. Cowling, "Thermal convection in magnetohydrodynamic boundary layers," *The Quarterly Journal of Mechanics and Applied Mathematics*, vol. 16, no. 1, pp. 1–15, 1963.

[3] M. Wahiduzzaman, R. Biswa, M. D. E. Ali, M. D. S. Khan, and I. Karim, "Numerical Solution of MHD Convection and Mass Transfer Flow of Viscous Incompressible Fluid about an Inclined Plate with Hall Current and Constant Heat Flux," *Applied Mathematics and Physics*, vol. 3, no. 12, pp. 1688–1709, 2015.

[4] G. S. Seth, R. Sharma, and S. M. Hussain, "Hall Effects on Unsteady MHD Natural Convection Flow of a Heat Absorbing Fluid Past an Accelerated Moving Vertical Plate with Ramped Temperature," *Emirates Journal for Engineering Research*, vol. 19, no. 2, pp. 19–32, 2014.

[5] G. S. Seth, S. M. Hussain, and S. Sarkar, "Effects of Hall current and rotation on unsteady MHD natural convection flow with heat and mass transfer past an impulsively moving vertical plate in the presence of radiation and chemical reaction," *Bulgarian Chemical Communications*, vol. 46, no. 4, pp. 704–718, 2014.

[6] G. S. Seth, and S. Sarkar, " MHD natural convection heat and mass transfer flow past a time dependent moving vertical plate with ramped temperature in a rotating medium with hall effects, radiation and chemical reaction," *Journal of Mechanics*, vol. 31, no. 1, pp. 91–104, 2015.

[7] L. K. Saha, M. A. Hossain and R. S. R. Gorla, " Effect of Hall current on the MHD laminar natural convection flow from a vertical permeable flat plate with uniform surface temperature," *International Journal of Thermal Sciences*, vol. 46, no. 8, pp. 790–801, 2007.

[8] L. K. Saha, S. Siddiqa, and M. A. Hossain, " Effect of Hall current on MHD natural convection flow from vertical permeable flat plate with uniform surface heat flux," *Applied Mathematics and Mechanics*, vol. 32, no. 9, pp. 1127–1146, 2011.

[9] M. Mahmood, S. Asghar, and M. A. Hossain, " Squeezed flow and heat transfer over a porous surface for viscous fluid," *Heat and Mass Transfer*, vol. 44, no. 2, pp. 165–173, 2007.

[10] S. Hussain, M. A. Hossain, and M. Wilson, " Natural convection flow from a vertical permeable flat plate with variable surface temperature and species concentration," *Engineering Computations*, vol. 17, no. 7, pp. 789–812, 2000.

[11] M. A. Hossain, S. K. Das, and I. Pop, "Heat transfer response of MHD free convection flow along a vertical plate to surface temperature oscillations," *International Journal of Non-Linear Mechanics*, vol. 33, no. 3, pp. 541–553, 1998.

[12] T. Cebeci and P. Bradshaw, *Physical and Computational Aspects of Convective Heat Transfer*, Springer-Verlag, New York, 1984.

[13] R. E. Bellman and R. E. Bradshaw, *Quasilinearization and Nonlinear Boundary-Value Problems*, Elsevier Publishing Company, New York, 1965.

[14] A. Raptis, " Radiation and free convection flow through a porous medium," *International Communications in Heat and Mass Transfer*, vol. 25, no. 2, pp. 289–295, 1998.

[15] S. S. Motsa, " Spectral relaxation method and spectral quasilinearization method for solving unsteady boundary layer flow problems," *Advances in Mathematical Physics*, Volume 2014, Article ID 341964, 12 pages, 2014. doi:10.1155/2014/341964.

[16] S. S. Motsa, F. G. Awad, Z. G. Makukula, and P. Sibanda," The Spectral Homotopy Analysis Method Extended to Systems of Partial Differential Equations," *Abstract and Applied Analysis*, Volume 2014, Article ID 241594, 11 pages, 2014. doi:10.1155/2014/241594.

[17] T. M. Agbaje, and S. S. Motsa, " Comparison between Spectral perturbation and Spectral relaxation approach for unsteady heat and mass transfer by MHD mixed convection flow over an impulsively stretched vertical surface with chemical reaction effect," *Journal of Interpolation and Approximation in Scientific Computing*, vol. 2015, no. 1, pp. 48–83, 2015. doi.org/10.5899/2015/jiasc-00076.

[18] L. N. Trefethen, *Spectral Methods in MATLAB*, SIAM, Philadelphia, 2000.

[19] C. Canuto, M. Y. Hussani, A. Quarteroni, and T. A. Zang, *Spectral Methods in Fluid Dynamics*, Springer-Verlag, Berlin, 1988.

[20] M. Li, and L. Wang, " Numerical Solution of Fractional Partial Differential Equation of Parabolic Type Using Chebyshev Wavelets Method," *Engineering Letters*, vol. 26, no. 2, pp. 224–227, 2018.

[21] G. Liu, Y. Luo, and L. Shu, " Asymptotic Synchronization of Complex Dynamical Networks with Time-Varying Delays on Time Scales," *Engineering Letters*, vol. 26, no. 2, pp. 210–215, 2018.

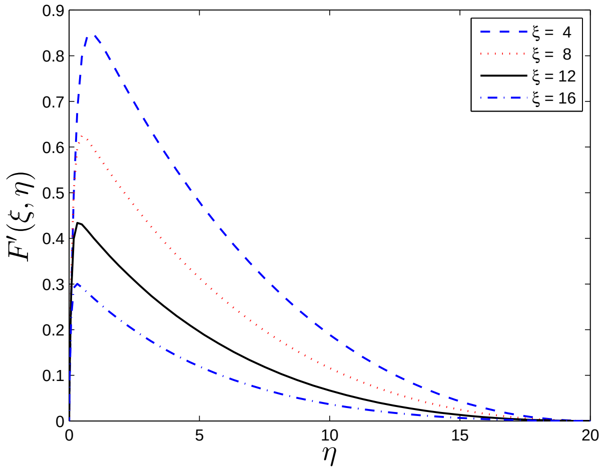

Fig. 2. Tangential velocity profile $F'(\xi,\eta)$ for different values of transpiration parameter ξ, when $M = 0.5$, $m = 2$, $Pr = 0.01$, $Sr = Sc = \delta = N_R = Df = 0$, and $He = 0$.

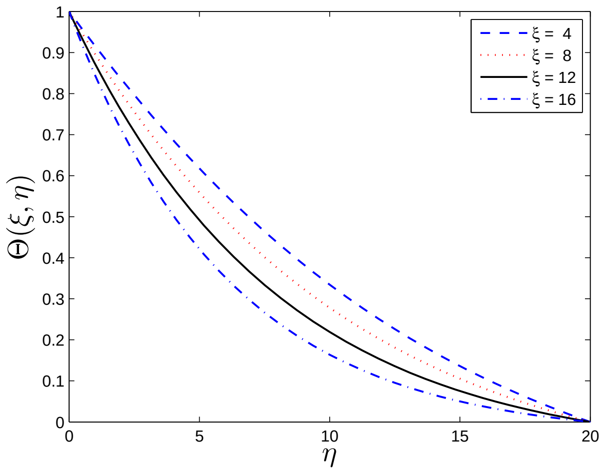

Fig. 3. Temperature profile $\Theta(\xi,\eta)$ for different values of transpiration parameter ξ, when $M = 0.5$, $m = 2$, $Pr = 0.01$, $Sr = Sc = \delta = N_R = Df = 0$, and $He = 0$.

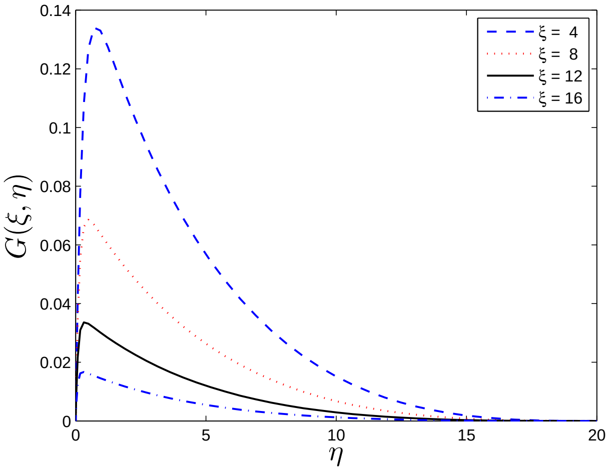

Fig. 4. Transverse velocity profile $G(\xi, \eta)$ for different values of transpiration parameter ξ, when $M = 0.5$, $m = 2$, $Pr = 0.01$, $Sr = Sc = \delta = N_R = Df = 0$, and $He = 0$.

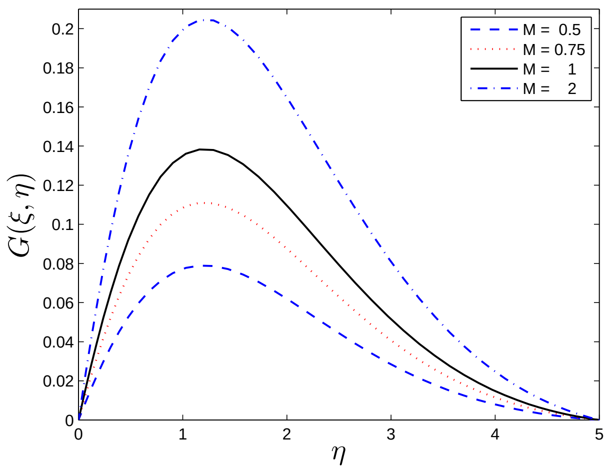

Fig. 6. Transverse velocity profile $G(\xi, \eta)$ for different values of magnetic field parameter M, when $\xi = 4$, $Sr = 0.6$, $Pr = 0.7$, $Df = 0.6$, $Sc = 1$, $m = 2$, $N_R = 0.2$, $\delta = 1$, and $He = 0.2$.

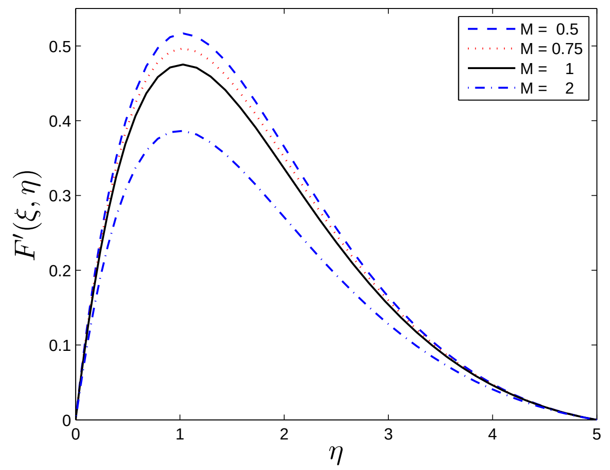

Fig. 5. Tangential velocity profile $F'(\xi, \eta)$ for different values of magnetic field parameter M, when $\xi = 4$, $Sr = 0.6$, $Pr = 0.7$, $Df = 0.6$, $Sc = 1$, $m = 2$, $N_R = 0.2$, $\delta = 1$, and $He = 0.2$.

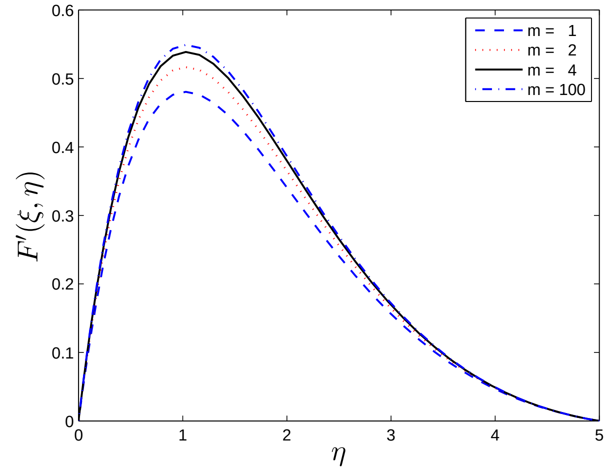

Fig. 7. Tangential velocity profile $F'(\xi, \eta)$ for different values of Hall parameter m, when $\xi = 4$, $Sr = 0.6$, $Pr = 0.7$, $Df = 0.6$, $Sc = 1$, $M = 0.5$, $N_R = 0.2$, $\delta = 1$, and $He = 0.2$.

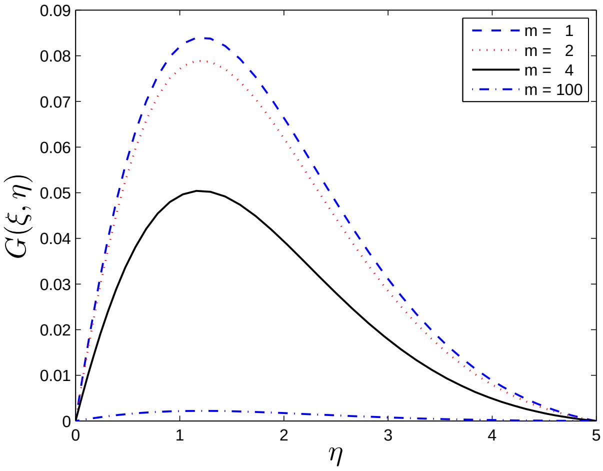

Fig. 8. Transverse velocity profile $G(\xi, \eta)$ for different values of Hall parameter m, when $\xi = 4$, $Sr = 0.6$, $Pr = 0.7$, $Df = 0.6$, $Sc = 1$, $M = 0.5$, $N_R = 0.2$, $\delta = 1$, and $He = 0.2$.

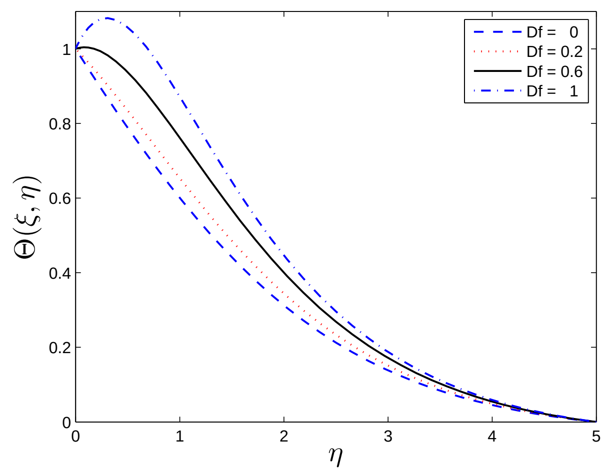

Fig. 9. Temperature profile $\Theta(\xi, \eta)$ for different values of Dufour number Df, when $\xi = 4$, $Sr = 0.6$, $Pr = 0.7$, $M = 0.5$, $Sc = 1$, $m = 2$, $N_R = 0.2$, $\delta = 1$, and $He = 0.2$.

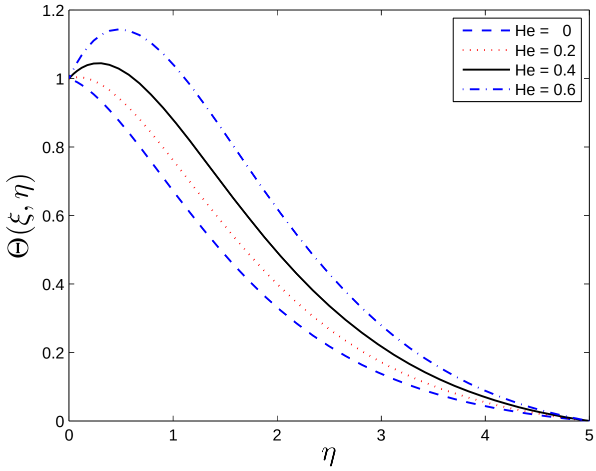

Fig. 10. Temperature profile $\Theta(\xi, \eta)$ for different values of heat generation parameter He, when $\xi = 4$, $Sr = 0.6$, $Pr = 0.7$, $M = 0.5$, $Sc = 1$, $m = 2$, $N_R = 0.2$, $\delta = 1$, and $Df = 0.6$.

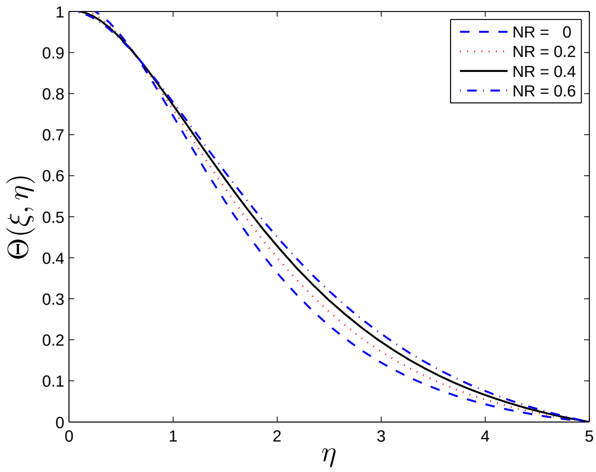

Fig. 11. Temperature profile $\Theta(\xi, \eta)$ for different values of radiation parameter N_R, when $\xi = 4$, $Sr = 0.6$, $Pr = 0.7$, $M = 0.5$, $Sc = 1$, $m = 2$, $He = 0.2$, $\delta = 1$, and $Df = 0.6$.

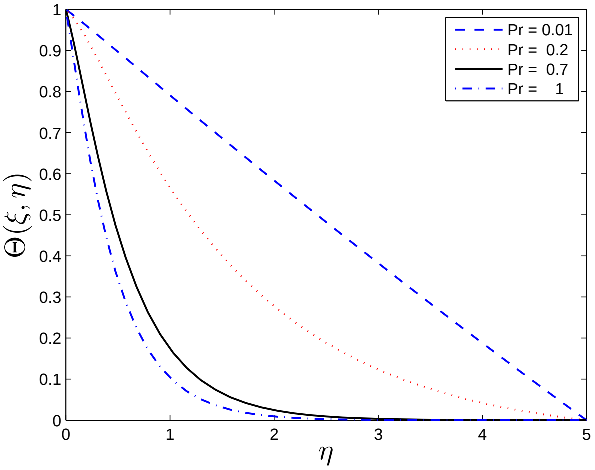

Fig. 12. Temperature profile $\Theta(\xi, \eta)$ for different values of Prandtl number Pr, when $\xi = 4$, $Sr = 0.6$, $N_R = 0.2$, $M = 0.5$, $Sc = 1$, $m = 2$, $He = 0.2$, $\delta = 1$, and $Df = 0.6$.

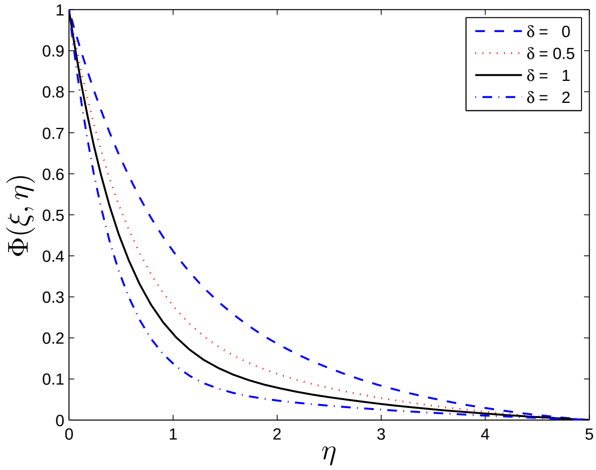

Fig. 14. Concentration profile $\Phi(\xi, \eta)$ for different values of chemical reaction parameter δ, when $\xi = 4$, $Pr = 0.7$, $N_R = 0.2$, $M = 0.5$, $Sc = 1$, $m = 2$, $He = 0.2$, $Sr = 0.6$, and $Df = 0.6$.

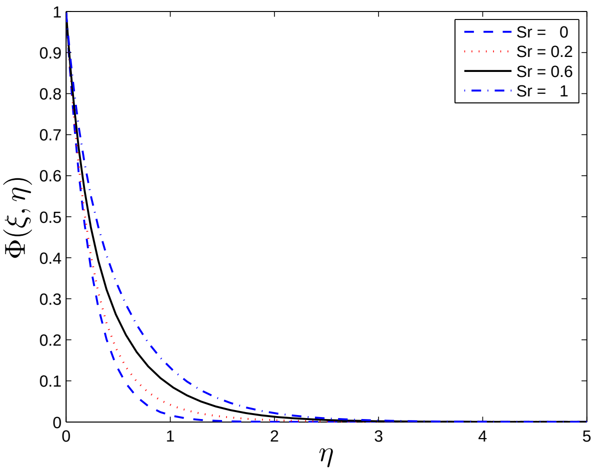

Fig. 13. Concentration profile $\Phi(\xi, \eta)$ for different values of Soret number Sr, when $\xi = 4$, $Pr = 0.7$, $N_R = 0.2$, $M = 0.5$, $Sc = 1$, $m = 2$, $He = 0.2$, $\delta = 1$, and $Df = 0.6$.

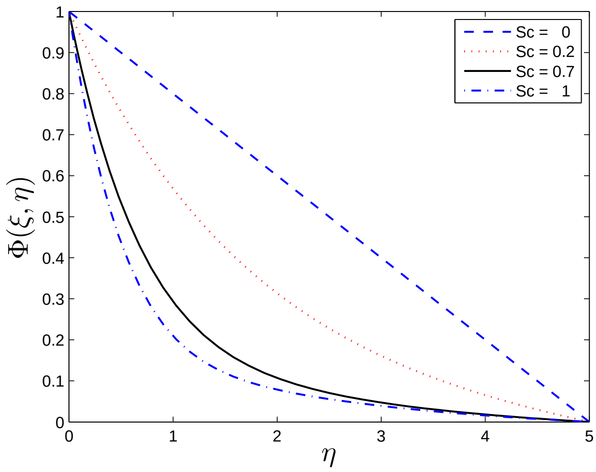

Fig. 15. Concentration profile $\Phi(\xi, \eta)$ for different values of Schmidt number Sc, when $\xi = 4$, $Pr = 0.7$, $N_R = 0.2$, $M = 0.5$, $\delta = 1$, $m = 2$, $He = 0.2$, $Sr = 0.6$, and $Df = 0.6$.

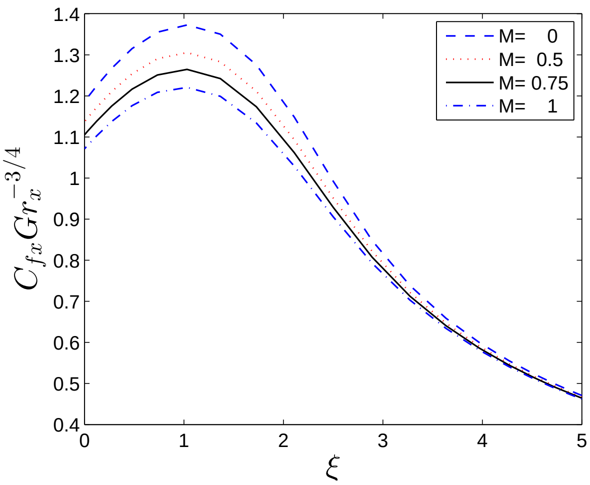

Fig. 16. Local skin-friction $C_{fx}Gr_x^{-3/4}$ for different values of Magnetic parameter M against transpiration parameter ξ, when $Pr = 0.7$, $N_R = 0.2$, $M = 0.5$, $\delta = 1$, $m = 2$, $He = 0.2$, $Sr = 0.6$, $Sc = 1$, and $Df = 0.6$.

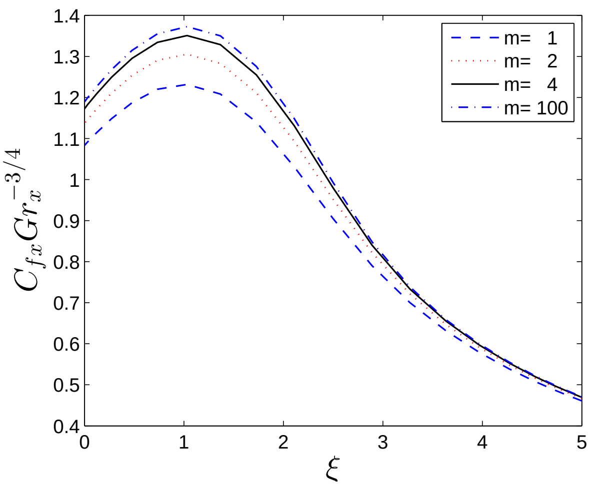

Fig. 17. Local skin-friction $C_{fx}Gr_x^{-3/4}$ for different values of Hall parameter m against transpiration parameter ξ, when $Pr = 0.7$, $N_R = 0.2$, $M = 0.5$, $\delta = 1$, $m = 2$, $He = 0.2$, $Sr = 0.6$, $Sc = 1$, and $Df = 0.6$.

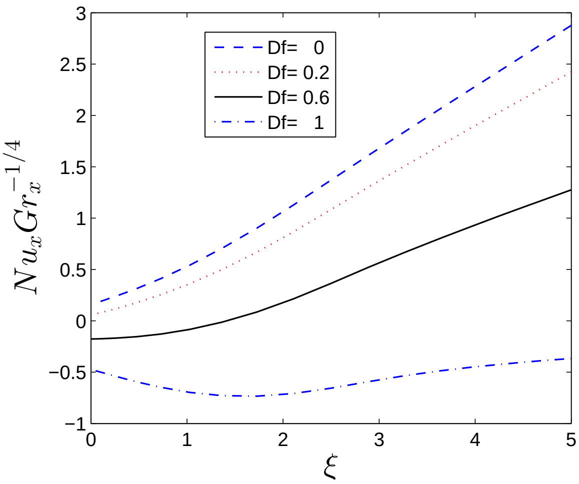

Fig. 18. Local Nusselt number $Nu_xGr_x^{-1/4}$ for different values of Magnetic parameter M against transpiration parameter ξ, when $Pr = 0.7$, $N_R = 0.2$, $M = 0.5$, $\delta = 1$, $m = 2$, $He = 0.2$, $Sr = 0.6$, $Sc = 1$, and $Df = 0.6$.

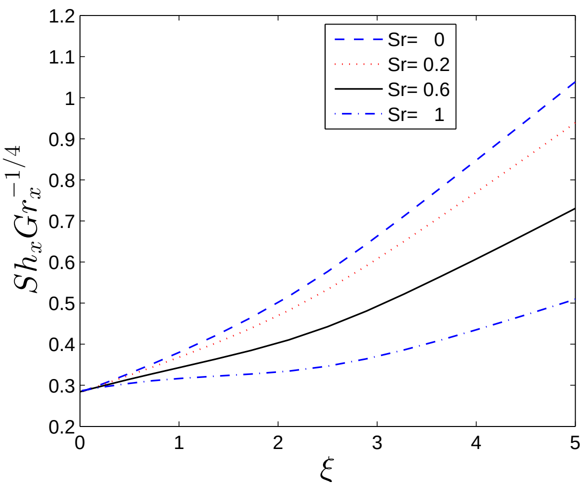

Fig. 19. Local Sherwood number $Sh_xGr_x^{-1/4}$ for different values of Hall parameter m against transpiration parameter ξ, when $Pr = 0.7$, $N_R = 0.2$, $M = 0.5$, $\delta = 0.2$, $m = 2$, $He = 0.2$, $Sr = 0.6$, $Sc = 0.2$, and $Df = 0.6$.

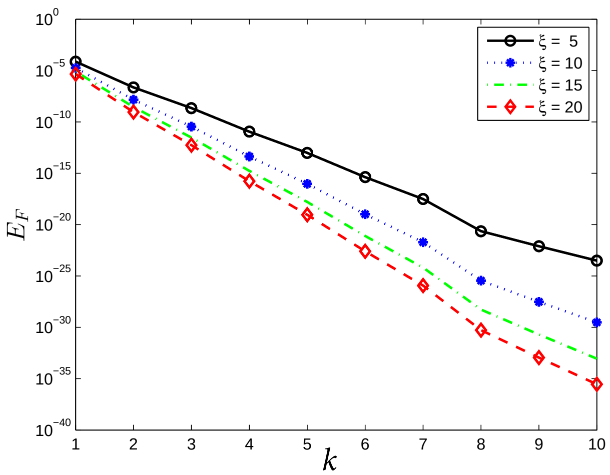

Fig. 20. Solution error E_F against increasing order (k) of LSPM series approximation for different values of transpiration parameter ξ, when $Pr = 0.7$, $N_R = 0.2$, $M = 0.5$, $\delta = 1$, $m = 2$, $He = 0.2$, $Sr = 0.6$, $Sc = 1$, and $Df = 0.6$.

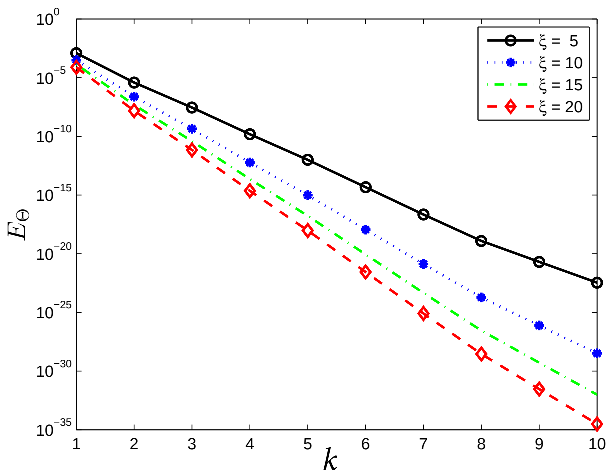

Fig. 22. Solution error E_Θ against increasing order (k) of LSPM series approximation for different values of transpiration parameter ξ, when $Pr = 0.7$, $N_R = 0.2$, $M = 0.5$, $\delta = 1$, $m = 2$, $He = 0.2$, $Sr = 0.6$, $Sc = 1$, and $Df = 0.6$.

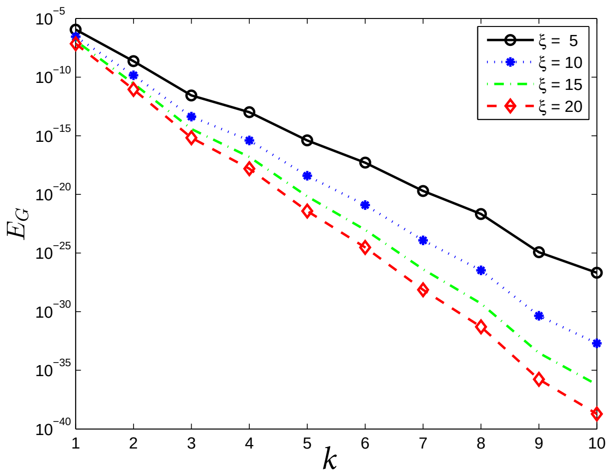

Fig. 21. Solution error E_G against increasing order (k) of LSPM series approximation for different values of transpiration parameter ξ, when $Pr = 0.7$, $N_R = 0.2$, $M = 0.5$, $\delta = 1$, $m = 2$, $He = 0.2$, $Sr = 0.6$, $Sc = 1$, and $Df = 0.6$.

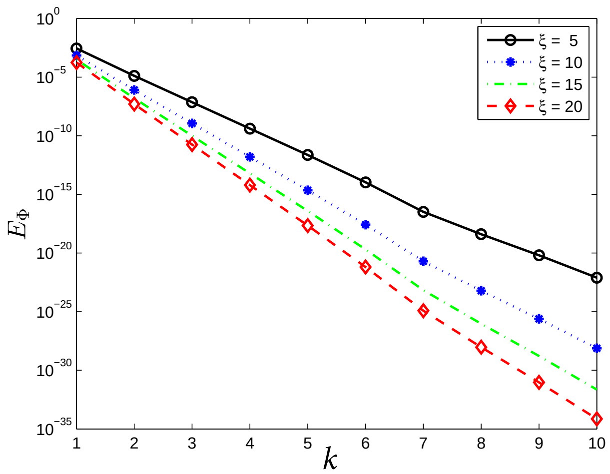

Fig. 23. Solution error E_Φ against increasing order (k) of LSPM series approximation for different values of transpiration parameter ξ, when $Pr = 0.7$, $N_R = 0.2$, $M = 0.5$, $\delta = 1$, $m = 2$, $He = 0.2$, $Sr = 0.6$, $Sc = 1$, and $Df = 0.6$.